Article:

Roach, LAN, White, DJ, Roberts, B et al. (1 more author) (2017) Initial 4D seismic results after CO 2 injection start-up at the Aquistore storage site. GEOPHYSICS, 82 (3). B95-B107. ISSN 0016-8033

https://doi.org/10.1190/geo2016-0488.1

Title: Initial 4D seismic results after CO_2 injection start-up at the Aquistore storage site

Authors: Lisa A. N. Roach[1], Don White[2], Brian Roberts[2], and Doug Angus[1].

Right Running Head: Aquistore CO_2 injection start-up results

[1] School of Earth and Environment, University of Leeds, Leeds, West Yorkshire United Kingdom. Email: l.a.n.roach@leeds.ac.uk; doug.angus@leeds.ac.uk

[2]Geological Survey of Canada, Ottawa, Ontario, Canada. Email: Don.White@canada.ca; Brian.Roberts@canada.ca.

Key words: 4D, time-lapse, seismic, CO_2 Storage, Aquistore, post-injection

ABSTRACT

The first post-CO_2-injection 3D time-lapse seismic survey was conducted at the Aquistore CO_2 storage site in February 2016 using the same permanent array of buried geophones employed for acquisition of 3 previous pre-CO_2 injection surveys from March 2012 to November 2013. By February 2016, 36 kilotonnes of CO_2 had been injected within the reservoir between 3170 m and 3370 m depth. We present time-lapse results from analysis of the first post-CO_2-injection data and 3 pre-CO_2-injection datasets. The objective of this analysis was to evaluate the ability of the permanent array to detect the injected CO_2. A '4D-friendly simultaneous' processing flow was applied to the data in an effort to maximize the repeatability between the pre- and post-CO_2-injection volumes while optimising the final subsurface image including the reservoir. Excellent repeatability was achieved amongst all surveys with GnRMS values of 1.13 to 1.19 for the raw prestack data relative to the baseline data which decreased during processing to GnRMS values of ~0.10 for the final cross-equalized migrated data volumes. A zone of high nRMS values (0.11-0.25 as compared to background values of 0.05-0.10) is identified within the upper Deadwood unit of the storage reservoir which likely corresponds to ~18 kilotonnes of CO_2. No significant nRMS anomalies are observed within the other reservoir units due to a combination of reduced seismic sensitivity, higher background nRMS values and/or small quantities of CO_2 residing within these zones.

INTRODUCTION

Aquistore is a CO_2 storage project located in southeastern Saskatchewan, Canada (Figure 1). It is one of the world's first commercial-scale CO_2 storage projects designed to demonstrate CO_2 storage in a deep saline aquifer. CO_2 is captured at SaskPower's Boundary

Dam coal-fired power plant and transported via pipeline to the storage site where it is injected into a brine-filled sandstone formation at ~3200 m depth.

The CO_2 storage monitoring programme at the Aquistore site includes a sparse areal permanent array of buried geophones (White et al., 2015; Roach et al., 2015) which was installed in an attempt to address the technical and operational requirements for monitoring the deep injection of CO_2. Sparse as used in this context means that the number of geophones (and/or shots) deployed per unit area over the survey area is small compared to a state-of-the-art 3D seismic survey with a temporary layout (White et al., 2015). Operationally, the sparse permanent array economizes the monitoring programme by minimizing costs due to mobilization and deployment efforts, by allowing use of the geophones for multiple purposes (e.g., controlled-source surveys and passive monitoring) and through the accommodation of flexible on-demand surveys. The technical advantage is the enhancement of data repeatability through the reduction of near-surface layer effects, the consistency of receiver coupling, the elimination of inter-survey positioning errors and an increase in signal-to-noise ratio.

3D time-lapse seismic monitoring has had widespread use in hydrocarbon reservoir management (Greaves and Fulp, 1987; Eastwood et al., 1994; Kalantzis et al., 1996; Lumley et al., 1997; Rickett and Lumley, 1998; Hirsche and Harmony, 1998; Johnston et al., 1998) and has been demonstrated as a powerful tool for the remote monitoring of physical changes in the subsurface due to the production and/or injection of fluids. More recently, 4D seismic methods have been successfully adapted for use in CO_2 reservoir monitoring (Arts et al., 2004; White et al., 2004; Mathieson et al., 2010; Urosevic et al., 2010; Eiken et al., 2011; Sato et al., 2011; Ivandic et al., 2012; Ringrose et al., 2013). The effectiveness of 4D seismic monitoring is influenced by the time-lapse seismic noise level (Aritman, 2001; Rickett and Lumley, 2001; Bakulin et al., 2007; Ma et al., 2009) and the change in reservoir parameters; i.e., the magnitude of rock property changes due to the presence of CO_2 (Lumley et al., 1997). Thus, an efficacious implementation of 4D monitoring requires the suppression of time-lapse noise which can be achieved by the repeatability of the acquisition procedure as closely as possible over different surveys (i.e., survey geometry as well as the duplication of the source and receiver characteristics) and the application of dedicated data processing methods (Meunier et al., 2001; Lumley et al., 2003; Calvert, 2005; Bakulin et al., 2007; Schisselé et al., 2009).

In this paper, we present the results of the first time-lapse analysis done after the start of CO_2 injection at the Aquistore storage site. One of the aims of this post-CO_2-injection analysis is to evaluate the ability of the sparse surface seismic data to detect and/or image the CO_2 plume after limited injection. To this end, the time-lapse analysis was performed using the first dataset acquired before injection (Baseline) and the only dataset acquired after CO_2 injection. In this study, we summarize the processing steps used in the simultaneous optimization of data repeatability and subsurface imaging. We also tracked the repeatability of the monitor seismic volumes as compared to the baseline seismic volume to ensure that the applied processing steps were effective. We then analysed the seismic amplitude differences in the context of the previously established background time-lapse noise at Aquistore. Finally, we evaluate the 3D time-lapse seismic results in light of the primary objective of monitoring which is to track the subsurface CO_2 plume at the site.

BACKGROUND

White et al. (2015), through a time-lapse analysis of two 3D dynamite seismic surveys acquired in March 2012 and May 2013 (Baseline and Monitor 1, respectively; both acquired prior to the start of CO_2 injection), demonstrated the technical advantages of a sparse buried permanent array. In their analysis, they compared dynamite data simultaneously recorded by buried and surface geophones; compared the repeatability of the raw permanent array time-lapse data to that acquired at the nearby Weyburn field using conventional methods; and compared the raw dynamite to a conventional high-resolution 3D Vibroseis survey recorded during the same acquisition period. Their analysis established that the use of the permanent array at the Aquistore site has achieved two significant results: (i) the reduction of the ambient noise level which is essential for sparse data acquisition, and (ii) the enhanced data repeatability which is vital to time-lapse imaging. They concluded that the high signal-to-noise level achieved in pre-CO_2-injection analysis (Baseline and Monitor 1) was due to the low level of ambient noise at the storage site, the use of sources (dynamite) and geophones that were deployed below the variable near-surface layer, and the use of dynamite sources which increased the signal-to noise-ratio by 20 dB relative to a Vibroseis source at the site (White et al., 2015). They also demonstrated that improvement in data repeatability achieved using the permanent array offsets the degradation in the time-lapse imaging associated with the lower fold data resulting from sparse acquisition.

The nRMS (normalised root-mean-square) difference is a metric for determining the similarity between two datasets and is defined as the RMS of the difference between traces of each vintage divided by the average RMS of the individual traces (Kragh and Christie, 2002). It can be calculated on a trace-by-trace basis or for the entire data set – we refer to the latter as the global nRMS or GnRMS. Theoretical nRMS values range from 0 to 2 – the datasets become more repeatable as the nRMS approaches 0. nRMS values of less than 0.2 are considered to be excellent under optimal 4D acquisition and processing practices (Lumley, 2010). In this paper, we use the nRMS to quantify the time-lapse noise.

The pre-CO_2-injection analysis (Baseline and Monitor 1) presented by Roach et al. (2015) provides evidence for the advantages of the permanent array – they demonstrated that the reduction in time-lapse noise achieved for the Aquistore raw data can be propagated through the full processing sequence to provide excellent repeatability in the final 3D data volumes. A GnRMS difference of 0.07 was achieved for the final processed volumes and establishes the background noise level at the Aquistore site. They also evinced the adequacy of a relatively simple processing flow in achieving the low nRMS values which is due to the high repeatability in the raw 3D seismic data.

It is this performance of the permanent array that has set the context for the post-CO_2-injection time-lapse analysis we present in this paper.

THE AQUISTORE CO_2 STORAGE SITE

The top of the CO_2 storage reservoir is located at a depth of 3130 m. The reservoir is a ~200 m thick clastic sequence that comprises the Cambro-Ordovician Winnipeg and Deadwood formations which lie unconformably above the Precambrian basement. The Winnipeg formation includes the ~15 m thick Icebox shale member which constitutes the reservoir caprock, and the underlying Black Island sandstone unit. The Middle Devonian Prairie Formation residing at 2515 m depth forms a secondary regional seal for CO_2 containment. It is a continuous evaporitic aquitard which is at least 150 m thick across the monitoring area (White et al., 2016).

CO_2 injection at the storage site began in April, 2015. Injection rates during the first year of operation have been variable, but rates of 400-600 tonnes/day have been typical since the fall of 2015. The first 3D time-lapse seismic survey (referred to as Monitor 3) since the start of CO_2 injection was conducted in February 2016. At the time of the survey, a total of 36,000 tonnes of CO_2 had been injected.

DATA ACQUISITION

The acquisition of the Monitor 3 3D seismic data was the third survey completed since the Baseline 3D survey of 2012 and was the first monitor survey acquired since the start of CO_2 injection in April 2015. Monitor surveys were also conducted in May 2013 (Monitor 1) and November 2013 (Monitor 2). The Monitor 2 survey was recorded during acquisition of a baseline 3D VSP (Harris et al., 2016). The Baseline and Monitor 1 surveys are described by Roach et al. (2015). For the Monitor 3 survey (Figure 1), 617 10 Hz vertical component geophones of the permanent seismic array recorded 679 dynamite shots during February 16 and 17. The geophones are buried at 20 m depth and the shots were detonated at 15 m depth to ensure that they were below the ground-water table.

The data were recorded using Geospace Seismic Recorders (GSRs) as was the case for all previous surveys. A large number of shot points were utilized as this was also the first Monitor 3D VSP survey which was being recorded simultaneously. A subset of these shots (~260 total) constituted the same shot points that had been used in all 3 previous 3D surface seismic surveys. Although the original grid of permanent geophones deployed in 2012 numbered 630, some have been lost due to farming activities, CO_2 pipeline easement, and well-site infrastructure. Of the 617 stations utilized for the Monitor 3 survey, 592 recorded data for all 679 shots. The primary causes for GSRs not recording data were battery failures, loss of GPS timing, and deployment errors. Table 1 lists the acquisition parameters of the Baseline and Monitor 3 surveys.

The receiver line spacing and station spacing were 144 m and 72 m, respectively, for the sparse array. Alternating geophone lines were staggered such that the receiver stations were shifted by 36 m on adjacent lines. The source points extended over a 3.0 km x 3.0 km area and shot lines for the surface 3D subset of shots were spaced at 288 m with an inline spacing of 144 m. Figure 1 shows the receiver and shot locations for the Monitor 3 survey. These acquisition parameters resulted in a nominal fold of ~40 for 36 m x 36 m bins. Low-fold data requires a maximization of signal-to-noise levels relative to the ambient noise as limited noise reduction can be achieved through stacking. The Monitor 3 survey was shot with 1 kg dynamite charges as was done with the previous surveys. Furthermore, using sources with constant characteristics (dynamite shot size and depth) generally produces a repeatable source wavelet.

Whereas the geophone locations are exactly the same for each seismic survey, the shot point locations are resurveyed and re-drilled for each seismic survey. For the first 3 seismic surveys, the shot hole positions were not resurveyed after drilling and thus the typical accuracy of the actual shot locations relative to the surveyed positions is somewhat uncertain. To assess this potential source of non-repeatability, the actual shot locations were resurveyed after drilling for the Monitor 3 seismic survey. It was found that 88% of the shot holes had actual locations that differed from the pre-drill positions by less than 3 m, and 99% were within 4 m of the original surveyed location. There was a single shot with a difference in post-drill and pre-drill locations of 7 m. Based on this evidence, we assume that the shot location uncertainties for the other seismic surveys are comparable.

DATA PROCESSING

Toward the goal of determining whether the CO_2 could be imaged after limited injection, we performed a time-lapse analysis between the Monitor 3 dataset and that acquired in March, 2012 prior to CO_2 injection – the Baseline. The principle of time-lapse seismic analysis lies in the assessment of the differences between seismic images that have been acquired at different instances. These differences reveal changes in the subsurface between the periods the images have been obtained. Thus, a processing flow that mitigates the time-lapse noise is a necessary complement to the optimized time-lapse data acquisition in order to produce the best time-lapse image of the subsurface.

Roach et al. (2015) devised a processing flow, influenced by that of Meadows and Cole (2013), which was capable of simultaneously maximizing the time-lapse repeatability between the Aquistore pre-CO_2-injection datasets (Baseline and Monitor 1) and optimizing the image of the reservoir and overburden. For the first objective, Roach et al. (2015) established that the "4D-friendly simultaneous" approach of processing was suitable for datasets from the Aquistore site. In this approach, each dataset is processed separately but with an identical processing sequence and parameters. The processing sequence included applying the same stacking and migration velocities to both datasets which is one method for reducing the misfit between positions of the imaged reflectors (Rickett and Lumley, 1998). For achieving the second processing objective, standard seismic processing tools were used.

We repeated the processing flow (Table 2) from Roach et al. (2015) on the post-injection (Baseline and Monitor 3) dataset in this time-lapse analysis adopting the same processing sequence and the same parameters, with two exceptions – the trace editing step was revised and horizon-based cross-correlation time shifts were applied to the post-stack cross-equalisation workflow. For trace editing we used a threshold nRMS criterion where the nRMS was computed within a 1300 ms window (700 ms to 2000 ms) for each shot-receiver trace pair of the nmo-corrected traces. Trace pairs having a nRMS value greater than 1.1 were removed from both datasets before subsequent processing. The 1.1 threshold represents a trade-off between the removal of poor (i.e., non-repeatable) traces and final trace count. At 1.1, most of the clearly visible poor traces were removed while a high trace count was maintained (i.e. 95% of the traces were kept (Table 3)). In the cross-correlation time shifts step, cross-correlation time-shifts were calculated using a 40 ms window centred on the Icebox horizon.

In the pre-stack processing sequence, dataset equalisation, which is the sorting of the Baseline and Monitor 3 datasets so that they have common shot, receiver and CDP trace pairs, resulted in each dataset having 134,724 common traces. In dataset equalisation, 19 shots and 54 receivers were discarded from the Baseline dataset while the number of shots and receivers removed from the Monitor 3 dataset were 427 and 16, respectively (see Table 3 for summary). Trace editing further reduced the trace count in each dataset to 129,159 common traces sorted into 242 common shots and 576 common receivers. CDP binning into 36 m x 36 m bins yielded 5819 bins with 79 inlines and 82 crosslines and a maximum fold of 85 (Figure 2). The post-stack processing sequence involved the cross-equalisation of the migrated Monitor 3 dataset to the migrated Baseline dataset (Table 2).

RESULTS

Figure 3 shows a vertical cross-section through the migrated Baseline volume along an inline that intersects the injection well. Superimposed onto the migrated volume is a log-based synthetic seismogram which shows a good tie to the wellbore geology. The resulting migrated Baseline image indicates that the processing flow applied to the data allowed the reservoir (at 3150 m to 3350 m depth or 1800 ms to 1900 ms) to be adequately imaged.

The refraction and residual statics as well as the surface consistent amplitudes (SCA) calculated for and applied to each dataset independently are shown in Figure 4. In the receiver domain, the refraction and residual statics, and the SCA corrections are very similar for both datasets. However, in the shot domain, whereas the refraction and residual static corrections are also similar, the SCA corrections differ – the mean SCA correction for the Baseline dataset is 0.02 whereas for the Monitor 3 dataset it is 0.03. Given that shot locations between the Baseline and Monitor 3 surveys were generally within 3 m, possible explanations may include changes in shot coupling or receiver coupling, degradation of the geophone response over time, changes in the near-surface that affect the effective source signature or geophone response (i.e., superposition of the direct and surface reflection).

The differences in the SCA values between both datasets is further highlighted in Figure 5 where a histogram of the SCA correction applied to each trace in the Baseline–Monitor 3 analysis is shown. The mean SCA correction applied to the Monitor 3 traces is a factor of 1.5 larger than the SCA correction applied to the Baseline traces.

The impact of processing on the repeatability of the Monitor 3 data relative to the Baseline data is shown at each step of processing in Figure 6 where the GnRMS value is plotted. Also shown for comparison are the GnRMS for the Baseline–Monitor 1 data and the Baseline–Monitor 2 analyses. This comparison confirms that the pre-CO_2-injection processing flow is also capable of increasing the similarity between the Baseline and Monitor 3 volumes.

For the post-CO_2-injection analysis, there is an overall decrease in the GnRMS as a function of processing step with a single exception – the application of t^2 gain to the trace edited datasets where the nRMS increased from 0.72 to 0.84 between the steps. The trace editing step has the largest impact on the repeatability between the datasets. The decrease in GnRMS after trace editing was 44%. The application of SCA also has a considerable effect where the GnRMS is almost halved – moving from 0.63 after the application of surface consistent deconvolution (SCD) to 0.32. Over the entire processing flow, the GnRMS decreased by 91%, a fall of 1.06 in the GnRMS of the raw dataset at 1.16 to the cross-equalised datasets at 0.10. Therefore, it is evident that the adopted processing flow capably increased the repeatability between the datasets with each step.

The post-migration cross-equalisation steps had very little effect on the repeatability between the datasets. Though the 4-step process increased the repeatability between the datasets, the change was only 0.02 (from 0.12 to 0.10) when the migrated datasets and the cross-equalised datasets were compared.

Figure 6 also elucidates the high degree of consistency over surveys with time through a comparison of the GnRMS from the Monitor 1 analysis with that of the Monitor 2 and Monitor 3 analyses. Comparing the GnRMS as a function of processing step for the Monitor 3 case to the pre-CO_2-injection cases, the trend observed is similar for all three analyses.

The repeatability between the raw traces for the pre- and post-CO_2-injection analysis is compared in Figure 7. Both datasets were winnowed so that the same trace pairs are used in the comparison. From the 127,089 traces used, the mean trace-by-trace nRMS was 0.58 for the Baseline–Monitor 1 pre-CO_2-injection datasets and 0.55 for the post-CO_2-injection datasets (computed within the 1300 ms window) while the GnRMS was 1.13 and 1.19 for the pre- and post-CO_2-injection, respectively. This 0.03 absolute difference in mean nRMS and 0.06 absolute difference in GnRMS between the periods at the raw data stage demonstrates that a low post-injection noise level (the same level of repeatability) was also achieved with the post-CO_2-injection survey.

The trace-by-trace nRMS of the raw traces as a function of shot-receiver pair, shown in Figure 8, provides a detailed comparison of the repeatability on a trace level pre- and post-CO_2-injection, and highlights how the nRMS varies with receiver shot pairs for each analysis. It also shows the percent difference between the nRMS of each shot-receiver trace pair of the Baseline–Monitor 1 pre-CO_2-injection and post-CO_2-injection raw datasets. On average, the difference in the raw shot-receiver trace pair nRMS between the survey pairs is 0.29. Figure 9 also compares the mean nRMS of each shot and each receiver for the pre- and post-CO_2-injection analyses which further highlights how similar the Monitor 1 dataset is to the Monitor 3 dataset – i.e., the repeatability between surveys at the storage site.

Figure 10 displays the spatial variation of the trace-by-trace nRMS for the Baseline–Monitor 1 pre-CO_2-injection and post-CO_2-injection stacked data at three stages of processing: trace edited, migrated and cross-equalised (see Table 2). As shown, the nRMS was calculated for a 100 ms window that includes the reservoir level to assess the repeatability within the zone of primary interest. As can be seen, the migration process significantly reduces the trace-to-trace variability in nRMS values. Also, the strong influence of stack fold is clear with nRMS values increasing substantially toward the edges of the volume. Both data vintages achieve very low nRMS values within the central part of the survey area with nRMS values in the range of 0.05-0.10.

The high degree of similarity between the final cross-equalized seismic volumes for the various vintages of data is illustrated in Figure 11 which shows an example section from the Baseline, Monitor 1, Monitor 2 and Monitor 3 seismic volumes. Any differences between these sections are clearly very subtle. Figure 12A-C shows the amplitude differences between the cross-equalised monitor datasets and the corresponding Baseline with the amplitudes scaled by a factor of 10 relative to the original data (see Figure 11). Also shown are corresponding sections of the RMS (Figure 12D-F) and nRMS (Figure 12G-I) amplitude differences calculated within a 10 ms sliding time window. Amplitude differences (Figure 12A-C) are observed at all levels within the section. The largest amplitude differences are observed toward the edges of either volume as would be expected based on the pattern of repeatability shown in Figure 10. Overall, the amplitude differences appear to be less pronounced on both pre-CO_2-injection surveys, although this is not the case at all depths. The decrease in data repeatability toward the edges of the section is also observed in the RMS and nRMS amplitudes (Figure 12D-I). In addition, the variable nature of repeatability with depth is also apparent. For example, inspection of Figures 12G-I reveals that the repeatability in the interval immediately above the reservoir (1700 ms to 1800 ms) has somewhat higher nRMS values overall than the reservoir interval (1800 ms to 1900 ms).

Focusing on the reservoir level and the central region of the images where the reliability is highest, there is an amplitude difference in the Monitor 3 section (Figure 12C) that straddles the CO_2 injection well at ~1850 ms to1860 ms that appears to be significant. This amplitude anomaly is not observed in the Monitor 1 or the Monitor 2 amplitude differences (Figure 12A,B). Also, it is more pronounced on the Monitor 3 RMS and nRMS sections (Figure 12F,I) where it clearly stands out relative to the background levels at this depth.

nRMS values for the Monitor 3 difference volumes are compared in Figure 13 for 3 levels of the reservoir along with corresponding nRMS values for the Monitor 1 and Monitor 2 difference volumes for reference. Inspection of the pre-CO_2-injection slices (left and middle columns) suggests that the data are most reliable for the upper two reservoir units (Black Island and upper Deadwood) as evidenced by the absence of spurious nRMS anomalies within the central region of the image. The lower Deadwood is less reliable as there are isolated zones where the nRMS values exceed 0.14. The pre-CO_2-injection maps provide a qualitative means of assessing the significance of the post-CO_2-injection nRMS changes. Using this as a guide, we conclude the following. 1) There are no significant nRMS changes detected within the Black Island unit. 2) Within the upper Deadwood unit, there is a 200 m-wide zone in the immediate vicinity of the injection well where nRMS values range from 0.10 up to 0.25 (Figure 13F). This anomaly is considered significant based on the reliability indicated by the Monitor 1 and Monitor 2 nRMS maps as well as the proximity to the injection well. 3) There are no significant nRMS changes near the injection well within the lower Deadwood unit. There are some large amplitude nRMS changes at distance from the injection well, but in each case, comparison with the corresponding Monitor 1 and Monitor 2 maps shows that these are zones of reduced reliability and thus are discounted as not being significant. In summary, the upper

Deadwood zone is the only interval for which the time-lapse seismic data clearly identify amplitude changes that are related to CO_2 injection.

DISCUSSION

The methodology used for data acquisition and processing of 3D time-lapse seismic data from the Aquistore site has proven to be robust. Including the Baseline and Monitor 1 surveys reported by Roach et al. (2015), we have now demonstrated excellent repeatability in 4 successive surveys over a period of 4 years. In each case, GnRMS values of 1.13-1.19 for the raw data are reduced during data processing to values of ~10%. Part of this consistency is certainly due to the use of a permanent array of buried geophones which demonstrably reduces the time-lapse noise (Roach et al., 2015; White et al., 2015). The repeatability of the dynamite sources might be expected to change with repeated use of the same approximate shot locations and associated mechanical damage to the subsurface. However, source repeatability has remained relatively consistent as was the experience from the Weyburn field over a period of 10 years (White, 2013). We attribute this largely to the fact that the shots are located below the water table.

The only post-injection amplitude/nRMS anomaly assessed as significant within the storage reservoir interval lies within the upper Deadwood interval. This is the reservoir interval where the predicted seismic capability for CO_2 detection is highest based on fluid substitution modelling by Roach et al. (2015, 2016). They concluded that the upper Deadwood unit (their Zone 2) should have the largest changes (by a factor of ~2) in seismic properties due to CO_2 replacing brine as compared to either the overlying Winnipeg Black Island unit (their Zone 1) or the lower Deadwood unit (their Zone 3). This includes the largest predicted changes in acoustic impedance (-17%) and Vp (-8%) in the upper Deadwood interval as compared to maximum changes in impedance of -8 to -9% and in Vp of -4 to -5% for the other two zones. Thus, the expected seismic detectability of CO_2 is highest for the upper Deadwood interval for a CO_2 saturated zone of a given thickness.

Figure 14 displays modelling results similar to those in Roach et al. (2015) but for actual perforation intervals within the reservoir. For zones of the same thickness (e.g., 2-12 m), higher nRMS values are achieved in the upper Deadwood interval as compared to the other intervals. This is generally true for low or high CO_2 saturations (e.g., 5% or 50%). For example, for a 10 m thick zone with 5% or 50% CO_2 saturation, the nRMS values in the upper Deadwood range from 1.3 to 1.6 times larger than for the other two zones. If CO_2 is distributed over the full depth extent of each interval, then higher nRMS values occur in the upper Deadwood and Black Island units as compared to the lower Deadwood interval.

The value of having a pre-CO_2-injection monitor survey (i.e., a Baseline and pre-CO_2-injection repeat survey) is clearly demonstrated in this study. Data repeatability and thus time-lapse reliability varies both laterally and vertically (e.g., see Figure 12) despite the best efforts to maximize repeatability during both data acquisition and processing. Having a pre-CO_2-injection monitor survey provides a measure of the non-repeatability of the time-lapse data in the absence of any injection-related effects and thus a measure of the general reliability of the data. The nRMS maps for the lower Deadwood unit demonstrate this point. Without the pre-CO_2-injection nRMS maps, the large nRMS anomalies observed away from the injection well would be difficult to evaluate based on the Monitor 3 data alone. But with these areas also showing up in the pre-CO_2-injection surveys as being less repeatable, they can be classified as spurious with some confidence.

The excellent repeatability (i.e., low nRMS values) achieved at that Aquistore site has a direct impact on the sensitivity of the time-lapse seismic data in detecting injected CO_2. The

Monitor 3 surface seismic was acquired as part of the first monitor VSP survey at the site and was not necessarily expected to image the relatively small amount of CO_2 (36 kilotonnes) that had been injected by that time. However, these results indicate that the surface time-lapse data is capable of detecting quantities of 36 kilotonnes or less at the reservoir depth of 3200 m. Downhole CO_2 flow measurements from a spinner survey indicate that 40% to 50% of the injected CO_2 is going into the upper Deadwood formation. From this we infer that the time-lapse image in the upper Deadwood may result from a CO_2 quantity of less than 18 kilotonnes. Conversely, there are likely significant amounts of CO_2 within the other 2 units (Black Island and lower Deadwood) that are not detected in the Monitor 3 data.

An assessment of the upper Deadwood amplitude anomaly can be made by direct comparison with the model nRMS values in Figure 14. Such a comparison should only provide minimum combined estimates of thickness and CO_2 saturation as the amplitude of the observed nRMS anomaly (Figure 13F) certainly underestimates its true amplitude due to the small lateral extent of this zone relative to the seismic wavelength (~100 m). Comparison of the nRMS peak amplitude value of 0.26 with Figure 14b shows that it would be consistent with either a 2 m thick zone with high saturation (>50%) or a 4 m thick zone with low saturation (<10%). That the CO_2 resides within a relatively thin zone is consistent with the absence of any significant nRMS difference immediately below the upper Deadwood anomaly. Otherwise, the time-delay introduced by propagation through the upper Deadwood zone would cause amplitude differences due to time-shifts at the deeper seismic horizons.

Simple volumetric calculations can be used to assess the areal extent of the upper Deadwood nRMS anomaly. However, it should be recognized that the areal extent of the observed nRMS anomaly likely underestimates the true extent of the CO_2 plume as mentioned above, but also because distal portions of the plume likely have lower CO_2 saturations and/or smaller thickness relative to the near-injection well zones rendering the associated seismic difference below the sensitivity threshold. Using a mean log-based porosity of 7% for the perforated injection intervals within the upper Deadwood sandstone (Table 3, Roach et al., 2015) and CO_2 density of 800 kg/m^3 (calculated for reservoir conditions of P=39 MPa and T=110° C), then 18 kilotonnes of CO_2 would occupy a cylindrical zone of minimum (i.e., 100% saturation) radius 101 m or 160 m (Figure 15), respectively, for a 10 m or 4 m thick zone. Flow simulations (Harris et al., 2016 and references therein) suggest CO_2 saturations are as high as 70-80% close to the injection well. At 50% saturation, the corresponding plume radius would be 143 m to 226 m. As can be seen in Figure 15, these area estimates for 18 kilotonnes are comparable to that of the observed upper Deadwood nRMS anomaly.

CONCLUSIONS

We have presented 3D time-lapse seismic results from the Aquistore CO_2 storage site including 3 pre-CO_2-injection surveys (Baseline, March 2012; Monitor 1, May 2013; Monitor 2, November 2013) and a post-CO_2-injection survey acquired in February, 2016. 36 kilotonnes of CO_2 had been injected from start-up in April, 2015 until February, 2016. From the processing and analysis of these data, we conclude the following:

1) The use of permanent buried geophones and buried dynamite sources has resulted in excellent repeatability between the 4 seismic surveys. The GnRMS for the raw prestack data ranges from 1.13 to 1.19 amongst the 3 monitor data sets relative to the baseline data set. The repeatability of the dynamite shots does not appear to have degraded over time, although a general reduction in data amplitudes is recorded for the last survey. The source of this difference, whether source- or receiver-related, is unknown. It may have to do with year-to-year variability in the near-surface.

2) Excellent GnRMS values are achieved for the final cross-equalized migrated data volumes through the application of the parallel processing flow from Roach et al. (2015). nRMS values in the central part of the Monitor data volumes lie in the range of 0.05 to 0.10 and the GnRMS values for the complete volumes are 0.10-0.12.

3) A significant amplitude difference (nRMS in the range of 0.11-0.25) is observed in the vicinity of the injection well within the upper Deadwood unit of the storage reservoir which likely corresponds to ~18 kilotonnes of CO_2. Log-based Gassmann fluid substitution modelling indicates that this interval has seismic properties that are more sensitive to the presence of CO_2 than the other reservoir injection zones. The area of the anomaly compares reasonably with the area of a 4-10 m thick cylindrical plume with radius of 101-160 m at 100% saturation. This represents a minimum size estimate as saturations are generally expected to be less than 70-80%.

4) No significant amplitude anomalies are observed within the other two CO_2 injection zones within the reservoir. Data repeatability within the Black Island sand is excellent and thus, even in light of the expected reduced seismic sensitivity in this zone, the seismic data suggests there is relatively little CO_2 within this zone. The data repeatability and seismic sensitivity for the lower Deadwood unit are not as high and thus we suggest that there is a significant quantity (< 18 kilotonnes) of CO_2 in this zone that is not detected seismically. The availability of a pre-CO_2 injection monitor survey was very useful in identifying spurious amplitude differences in the post- CO_2 injection monitor survey.

These time-lapse seismic results will be utilized in assessing the predictions of CO_2 distribution based on fluid flow simulations for the site.

ACKNOWLEDGEMENTS

The authors wish to thank the Petroleum Technology Research Centre and SaskPower. Funding for the permanent array was in part provided by the ecoEII Program of Natural Resources Canada. GSC contribution no. 20140197. The authors would also like to acknowledge the financial support of the UK CCS Research Centre (www.ukccsrc.ac.uk) in carrying out this work. The UKCCSRC is funded by the EPSRC as part of the RCUK Energy Programme. This research was also funded by the EPSRC Geological Storage consortium DiSECCS (EP/K035878/1) and EPSRC Early Career Fellowship (EP/K021869/1) held by DA and the EPSRC.

REFERENCES

Aritman, B.C., 2001, Repeatability study of seismic source signatures: Geophysics, **66**, 1811–1817.

Arts, R., O. Eiken, R.A. Chadwick, P. Zweigel, L. van der Meer, and G.A. Kirby, 2004, Monitoring of CO_2 injected at Sleipner using time-lapse seismic data: Energy, **29**, 1383 – 1393.

Bakulin, A., J. Lopez, I.S. Herhold, and A. Mateeva, 2007, Onshore monitoring with virtual-source seismics in horizontal wells: Challenges and solutions: 77th Annual International Meeting, SEG, Expanded Abstracts, 2893–2897.

Calvert, R.C., 2005, Insights and methods for 4D reservoir monitoring and characterization: 2005 Distinguished Instructor Short Course, Distinguished Instructor Series, **8**, SEG, Tulsa.

Eastwood, J., P. Lebel, A. Dilay, and S. Blakeslee, 1994, Seismic monitoring of steam-based recovery of bitumen: The Leading Edge, **13(4)**, 242-251.

Eiken, O., P. Ringrose, C. Hermanrud, B. Nazarian, T. A. Torp, and L. Høier, 2011, Lessons learned from 14 years of CCS operations: Sleipner, In Salah and Snøhvit: Energy Procedia, **4**, 5541-5548.

Greaves, R.J., and T.J. Fulp, 1987, Three-dimensional seismic monitoring of an enhanced oil recovery process: Geophysics, **52**, 1175-1187.

Harris, K., D. White, D. Melanson, C. Samson, and T. Daley, 2016, Feasibility of Time-lapse VSP Monitoring at the Aquistore CO2 Storage Site Using a Distributed Acoustic Sensing System: International Journal of Greenhouse Gas Control, **50**, 248-260, http://dx.doi.org/10.1016/j.ijggc.2016.04.016.

Hirsche, K.W., and B. Harmony, 1998, Time-lapse seismic monitoring of a SE Asian field—A case history: 68th Annual International Meeting, SEG, Expanded Abstracts, 24–26.

Ivandic, M., C. Yang, S. Lüth, C. Cosma, and C. Juhlin, 2012, Time-lapse analysis of sparse 3D seismic data from the CO2 storage pilot site at Ketzin, Germany: Journal of Applied Geophysics, **84**, 14-28.

Johnston, D. H., R. S. McKenny, J. Verbeek, and J. Almond, 1998, Time-lapse seismic analysis of Fulmar Field: The Leading Edge, **17**, 1420, 1422–1426, 1428.

Kragh, E., and P. Christie, 2002, Seismic repeatability, normalized rms, and predictability: The Leading Edge, **21**, 640–647, doi: http://dx.doi.org/10.1190/1.1497316.

Kalantzis, F., A. Vafidis, E.R. Kanasewich, and A. Kostyukevich, 1996, Seismic monitoring and modeling of an enhanced oil recovery project at Cold Lake, Alberta, Canada: Canadian Journal of Exploration Geophysics, **32**, 77-89.

Lumley, D. E., R. A. Behrens, and Z. Wang, 1997, Assessing the Technical Risk of a 4D Seismic Project: The Leading Edge, **16**, 1287–1291.

Lumley, D. E., D. C. Adams, M. A. Meadows, and S. P. Cole, 2003, 4D seismic data processing issues and examples: 73rd Annual International Meeting, SEG, Expanded Abstracts, 1394–1397.

Lumley, D. E, 2010, 4D seismic monitoring of CO2 sequestration: The Leading Edge, **29**,150-155.

Ma J., L. Gao, and I. Morozov, 2009, Time-lapse repeatability in 3C-3D dataset from Weyburn. CO2 sequestration project: CSPG CSEG CWLS Convention, Expanded Abstracts, 255–258.

Mathieson, A., J. Midgley, K. Dodds, I. Wright, P. Ringrose, and N. Saoula, 2010, CO2 sequestration monitoring and verification technologies applied at Krechba, Algeria: The Leading Edge, **29**, 216–221.

Meadows, M. A., and S. P. Cole, 2013, 4D seismic modeling and CO2 pressure-saturation inversion at the Weyburn Field, Saskatchewan: International Journal of Greenhouse Gas Control, **16**, S103–S117, doi:10.1016/j.ijggc.2013.01.030.

Meunier J., F. Huguet, and P. Meynier, 2001, Reservoir monitoring using permanent sources and vertical receiver antennae: The Cere-la-Ronde case study: The Leading Edge, **20**, 622–629.

Rickett, J., and D. E. Lumley, 1998, A cross-equalization processing flow for off-the-shelf 4-D seismic data: 68th Annual International Meeting, SEG, Expanded Abstracts, 16–19.

Rickett, J. E., and D. E. Lumley, 2001, Cross-equalization data processing for time-lapse seismic reservoir monitoring: A case study from the Gulf of Mexico: Geophysics, **66**, 1015–1025.

Ringrose, P. S., A. S. Mathieson, I. W. Wright, F. Selama, O. Hansen, R. Bissell, N. Saoula, and J. Midgley, 2013, The In Salah CO2 Storage Project: Lessons Learned and Knowledge Transfer: Energy Procedia, **37**, 0, 6226-6236.

Roach, L. A. N., D. J. White, and B. Roberts, 2015, Assessment of 4D seismic repeatability and CO_2 detection limits using a sparse permanent land array at the Aquistore CO2 storage site: Geophysics, **80(2)**, WA1-WA13. doi:10.1190/geo2014-0201.1

Roach, L.A.N., D.A.C. Angus, and D.J. White, 2016, Assessment of the limitations on the seismic detectability of injected CO_2 within a deep geological reservoir. Energy Procedia, (in Press).

Sato, K., S. Mito, T. Horie, H. Ohkuma, H. Saito, J. Watanabe, and T. Yoshimura, 2011, Monitoring and simulation studies for assessing macro- and meso-scale migration of CO2 sequestered in an onshore aquifer: Experiences from the Nagaoka pilot site, Japan: International Journal of Greenhouse Gas Control, **5**, 125-137.

Schissele, E., E. Forgues, J. Echappé, J. Meunier, O. de Pellegars, and C. Hubans, 2009, Seismic repeatability — Is there a limit?: 71st Annual International Conference and Exhibition, EAGE, Extended Abstracts, **V021**.

Urosevic, M., R. Pevzner, A. Kepic, P. Wisman, V. Shulakova, and S. Sharma, 2010, Time-lapse seismic monitoring of CO_2 injection into a depleted gas reservoir – Naylor Field, Australia: The Leading Edge, **29**,164–169.

White, D., 2013, Seismic characterization and time-lapse imaging during seven years of CO2 flood in the Weyburn field, Saskatchewan, Canada: International Journal of Greenhouse Gas Control, **16**, S78–S94, doi: http://dx.doi.org/10.1016/j.ijggc.2013.02.006

White, D.J., G. Burrowes, T. Davis, Z. Hajnal, K. Hirsche, I. Hutcheon, E. Majer, B. Rostron, and S. Whittaker, 2004, Greenhouse gas sequestration in abandoned oil reservoirs: International Energy Agency Weyburn pilot project GSA Today, **14**, 4–10.

White, D.J., L.A.N. Roach, and B. Roberts, 2015, Time-lapse seismic performance of a sparse permanent array: Experience from the Aquistore CO2 storage site: Geophysics, **80(2)**, WA35-WA48, doi: 10.1190/geo2014-0239.1.

White, D., Hawkes, C., and Rostron, B., 2016, Geological characterization of the Aquistore CO2 storage site from 3D seismic data: International Journal of Greenhouse Gas Control, **54(1)**, 330-344, doi:10.1016/j.ijggc.2016.10.001.

Table 1: Acquisition parameters for the 3D seismic surveys.

Parameters	Baseline	Monitor 3
Survey Date	March, 2012	February, 2016
Receivers		
Type	10 Hz vertical component geophone (GSR*)	
Spatial coverage	2.5 km x 2.5 km	
Depth of burial	20 m	
No. of receiver lines	18	
No. of station per line	35	
Receiver line spacing	144 m	
Receiver spacing	72 m	
No. of Receivers	630	592
Sources		
Type	Dynamite	
Spatial coverage	3 km x 3 km	
Charge depth	15 m	
Charge size	1 kg	
No. of shot lines	12	
No. of stations per line	22	
Shot line spacing	288 m	
Shot station spacing	144 m	
No. of shots	261	679

* Geospace Seismic Recorder

Table 2: List of processing steps applied to each dataset.

Processing Steps	Fig.6 Abbr.
Pre-Stack	
Dataset Equalisation	Raw
Trace Edit	TrEd
t^2 amplitude Scaling	Gain
Surface Consistent Amplitude Balancing (source, receiver and offset decomposition)	SCA
Bandpass Filtering (Ormsby 10-15-90-100 Hz)	BPF
Surface Consistent Spiking Deconvolution (source and receiver decomposition)	SCD
Bandpass Filtering (10-15-90-100 Hz)	
Refraction Statics (datum:600m, replacement velocity=2200m/s , initial weathering velocity = 1200 m/s)	Refr
2 Pass Velocity Analysis (576m x 576m)	
2 Pass Surface Consistent Residual Statics (1500 ms-2000 ms window)	Res
NMO correction (30% stretch mute, 2nd Pass velocity function)	
CDP stacking (single stacking velocity function)	
Least squares interpolation (18m x 18m bins)	Intp
Explicit 3D Finite Difference Migration	Mig
Post-stack XE (window: 700 ms-2000 ms)	
Phase-Time matching	PhTm
Shape filtering	PTSh
Amplitude normalisation	PTSN
Horizon-based XE time shifts (40ms window centred on Black Island)	HBCT

Table 3: Summary of dataset statistics.

Dataset		Baseline	Monitor 3
Original	Traces	164,430	401,968
	Shots	261	679
	Receivers	630	592
Raw (winnowed)	Traces	134,724	
	Shots	242	
	Receivers	576	
Trace Edit	Traces	129,159	
	Shots	242	
	Receivers	576	

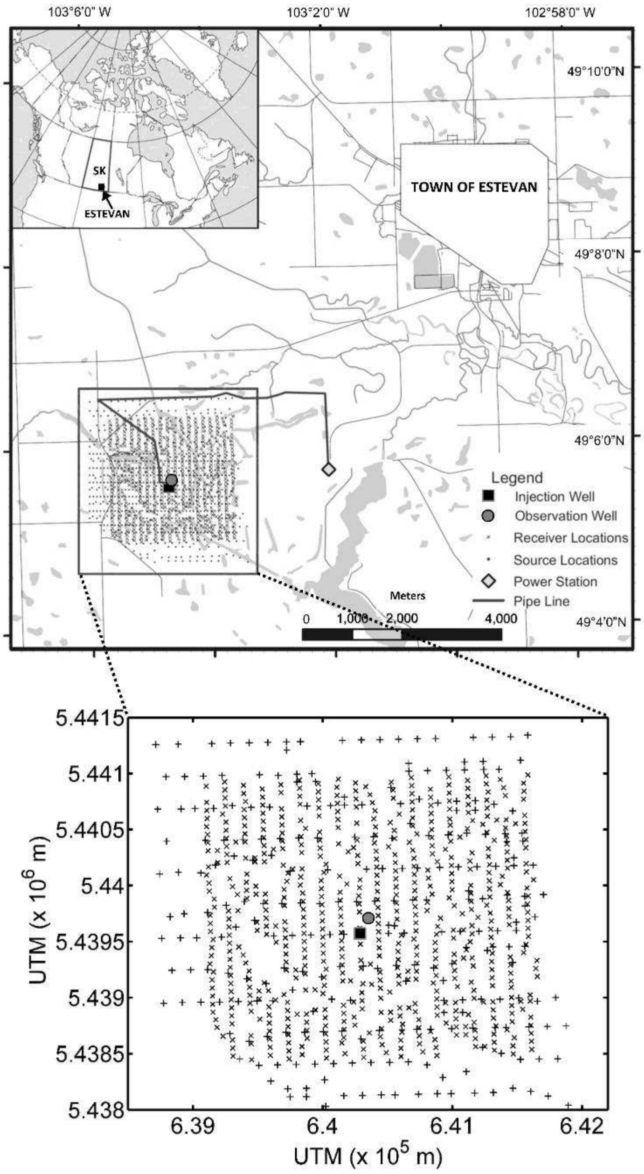

Figure 1: Monitor 3 survey geometry. Shots locations are marked with '+' and receiver locations are marked with 'x'. The injection well is marked with a gray-outlined black square and the observation well is marked with a black-outlined grey circle.

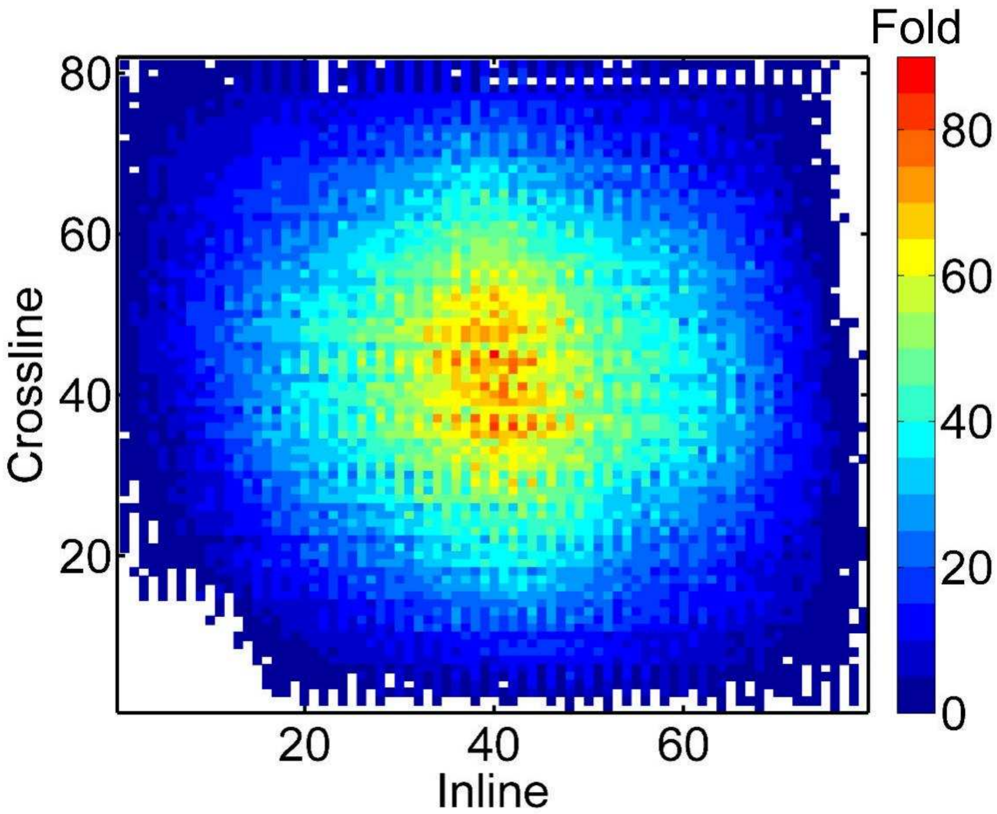

Figure 2: Fold of the Baseline and Monitor 3 datasets after winnowing.

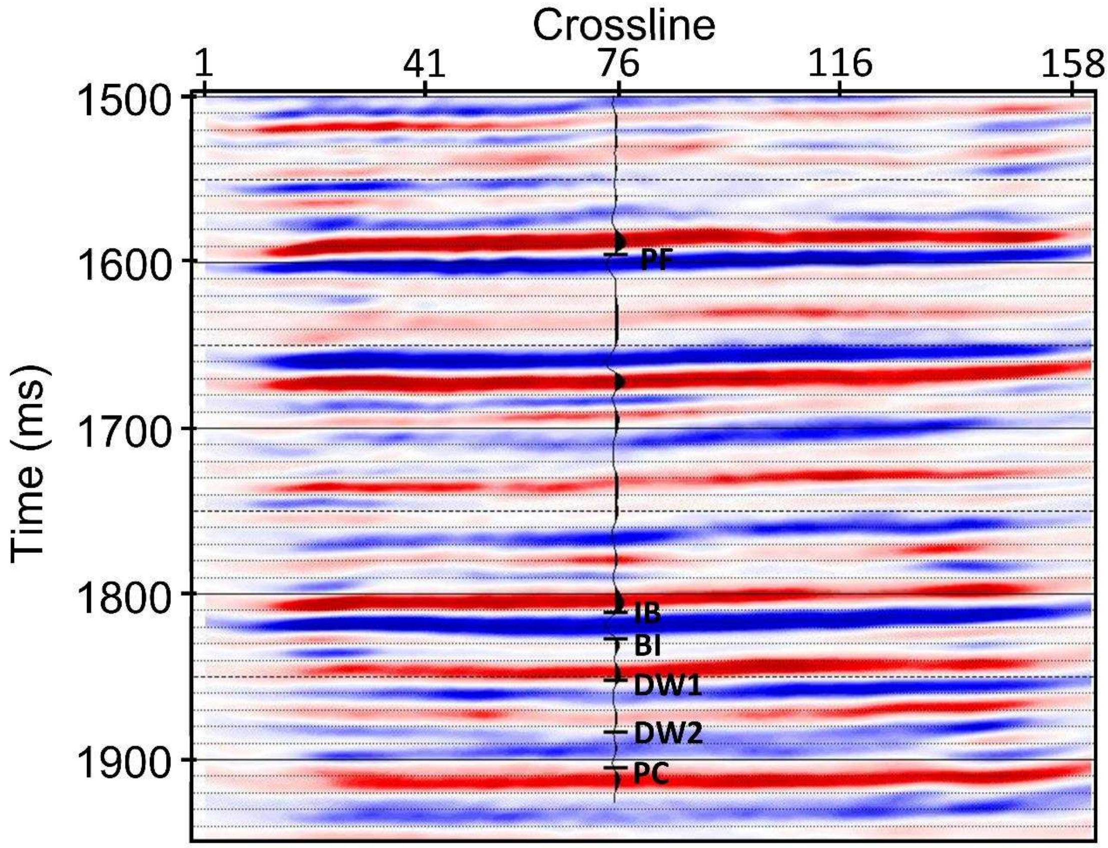

Figure 3: Cross-section through time migrated baseline dataset along an inline that intersects the injection well. The inserted wiggle trace is a log-based 1D synthetic seismogram created using a wavelet extracted from the data. The crossline spacing is 18 m (due to interpolation prior to migration). The labelled reservoir horizons are: IB=Icebox shale, BI=Black Island sandstone, DW1=upper Deadwood Formation, DW2= lower Deadwood Formation, PC=Precambrian. Also labelled is the secondary regional seal: PF=Prairie formation.

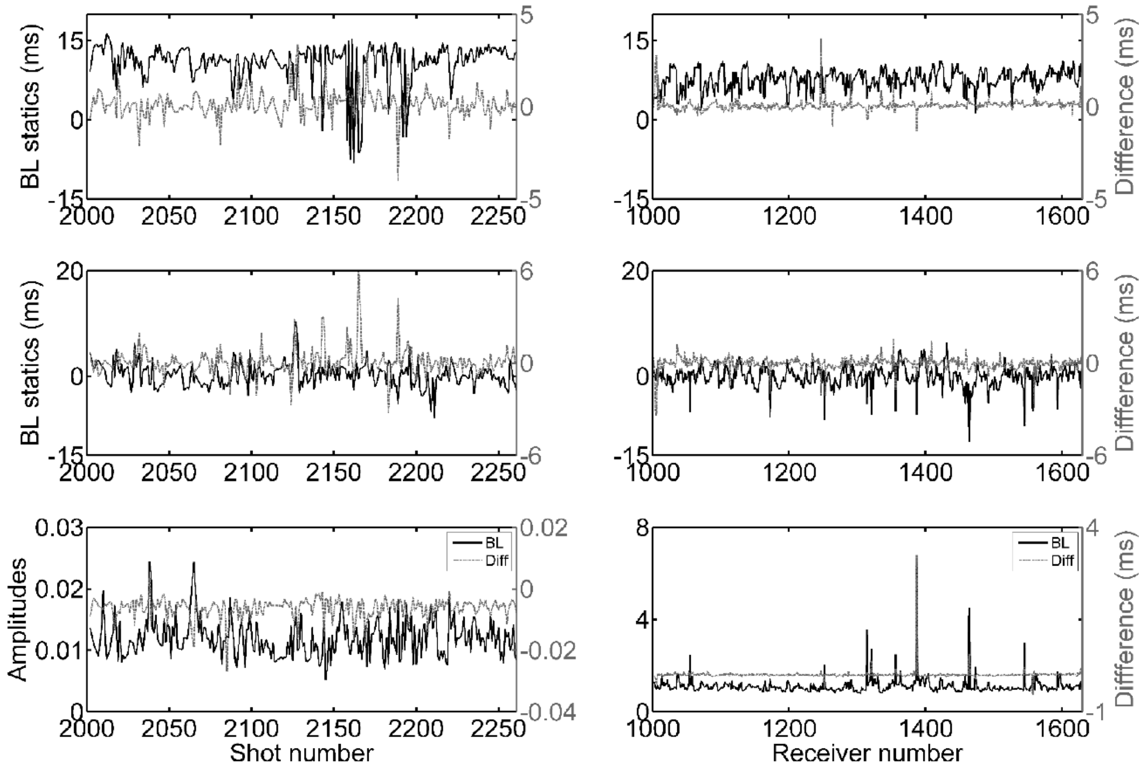

Figure 4: Source and receiver statics and surface consistent amplitudes. (A) Source and (B) receiver refraction statics; (C) source and (D) receiver residual statics; and the surface consistent amplitudes for (E) sources and (F) receivers. The Baseline dataset values are marked with black lines in all plots, whereas the difference between the Baseline and Monitor 3 values are marked with grey lines. Left column shows the shot statics and amplitudes while the right column shows the same for the receivers.

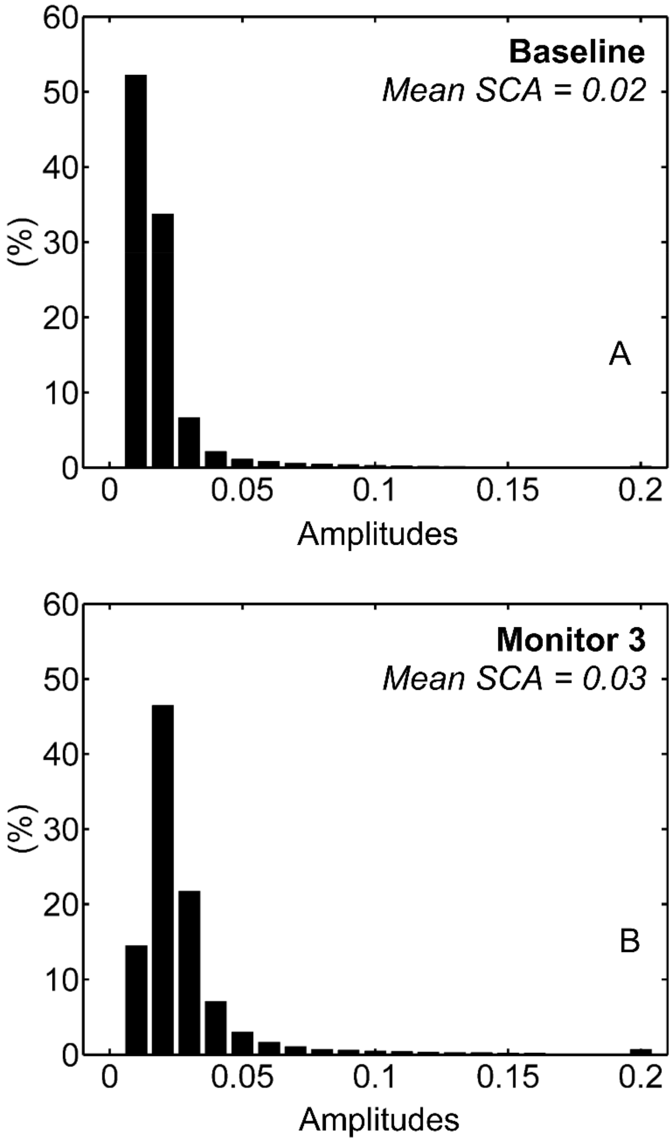

Figure 5: Surface consistent amplitudes computed within a 1300ms window (700 ms to 2000 ms) for the winnowed (A) Baseline and (B) Monitor 3 datasets. Monitor 3 amplitudes are 1.5 times larger than the baseline’s.

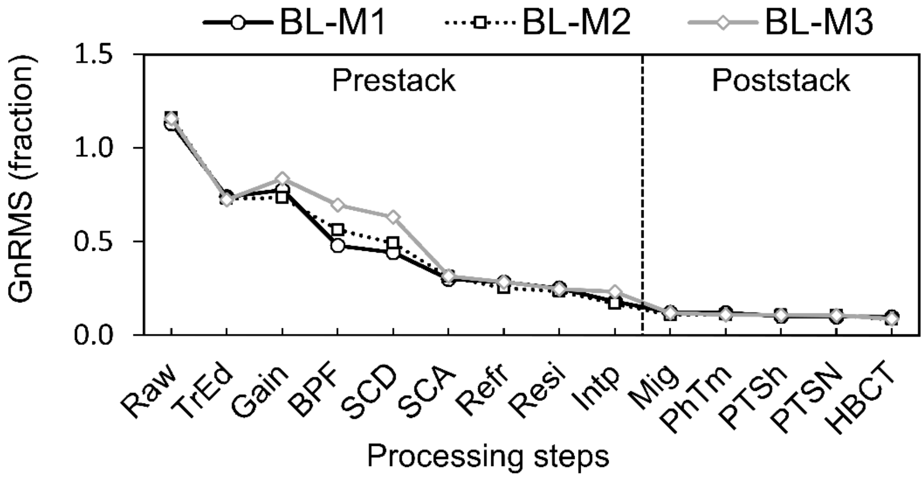

Figure 6: Global nRMS computed within the window 700 ms to 2000 ms on stacked traces for post-CO_2-injection and pre-CO_2-injection datasets. Each processing step is described in Table 2.

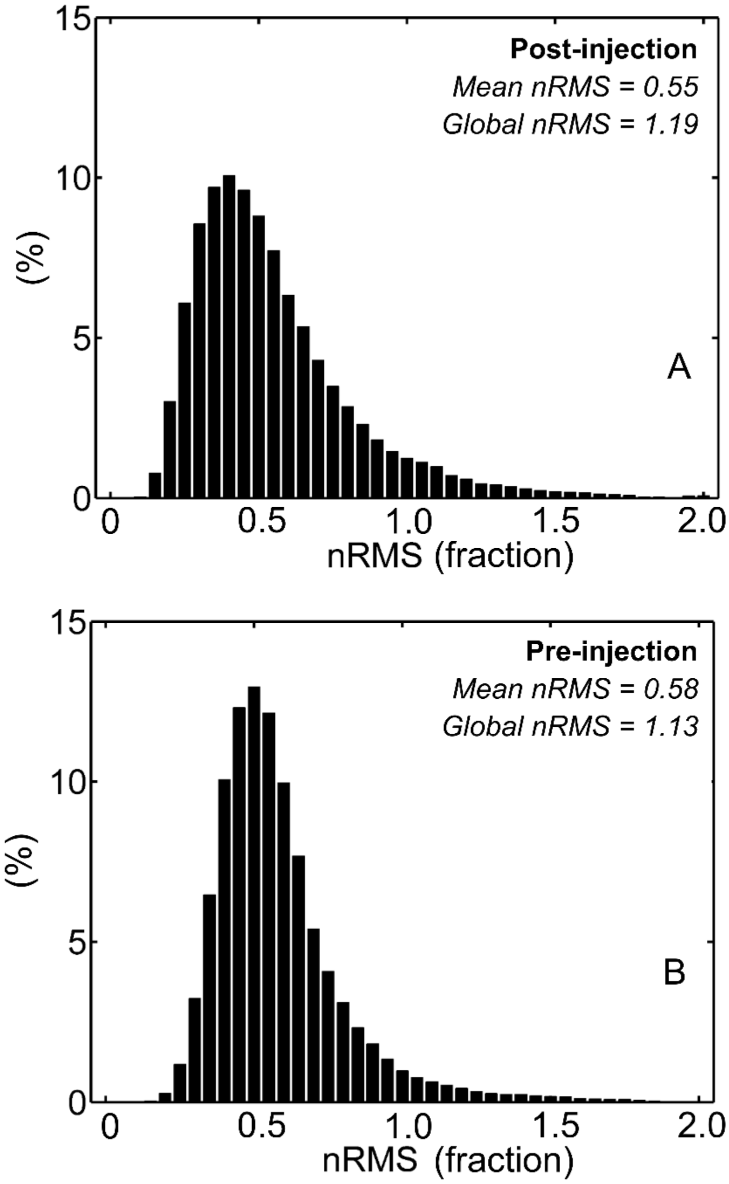

Figure 7: Histograms of the trace-by-trace nRMS computed within window 700 ms to 2000 ms on the nmo-corrected raw (un-processed) traces for (A) Baseline–Monitor 3 (post-CO_2-injection) shot-receiver trace pairs and (B) Baseline–Monitor 1 (pre-CO_2-injection) shot-receiver trace pairs. Each dataset has common shot-receiver trace pairs.

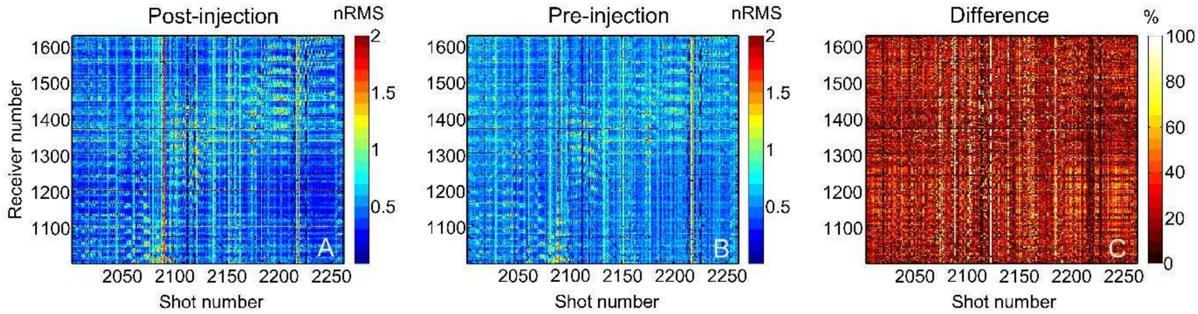

Figure 8: Maps of the trace-by-trace nRMS of the (A) Baseline–Monitor 3 (post-CO_2-injection) and (B) Baseline–Monitor 1 (pre-CO_2-injection) datasets for each shot-receiver trace pair, and (C) the percent difference between these two maps. The nRMS was computed within window 700 ms to 2000 ms on the nmo-corrected raw (un-processed) trace pairs. The pre- and post-CO_2-injection datasets have common shot-receiver trace pairs.

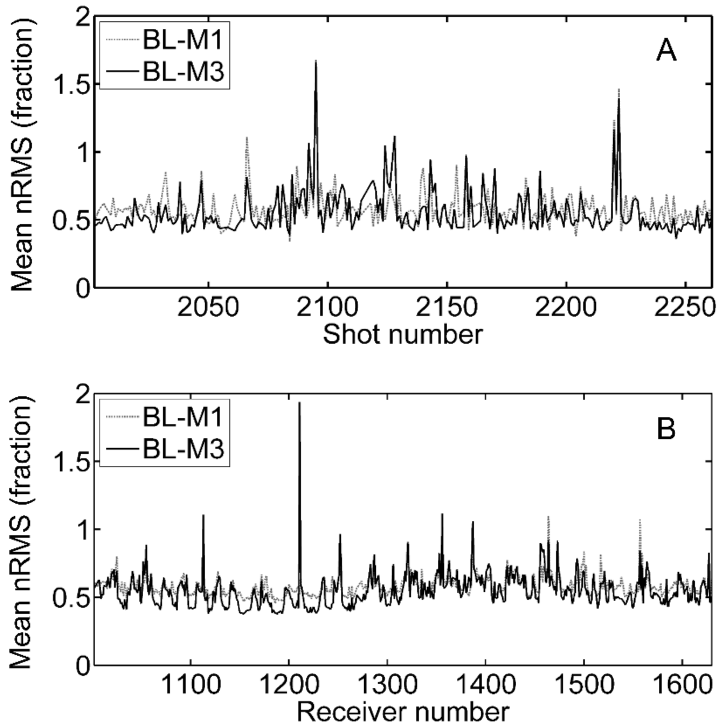

Figure 9: A comparison of the (A) shot and (B) receiver mean nRMS for the Baseline–Monitor 1 pre- and Baseline–Monitor 3 post-CO_2-injection datasets.

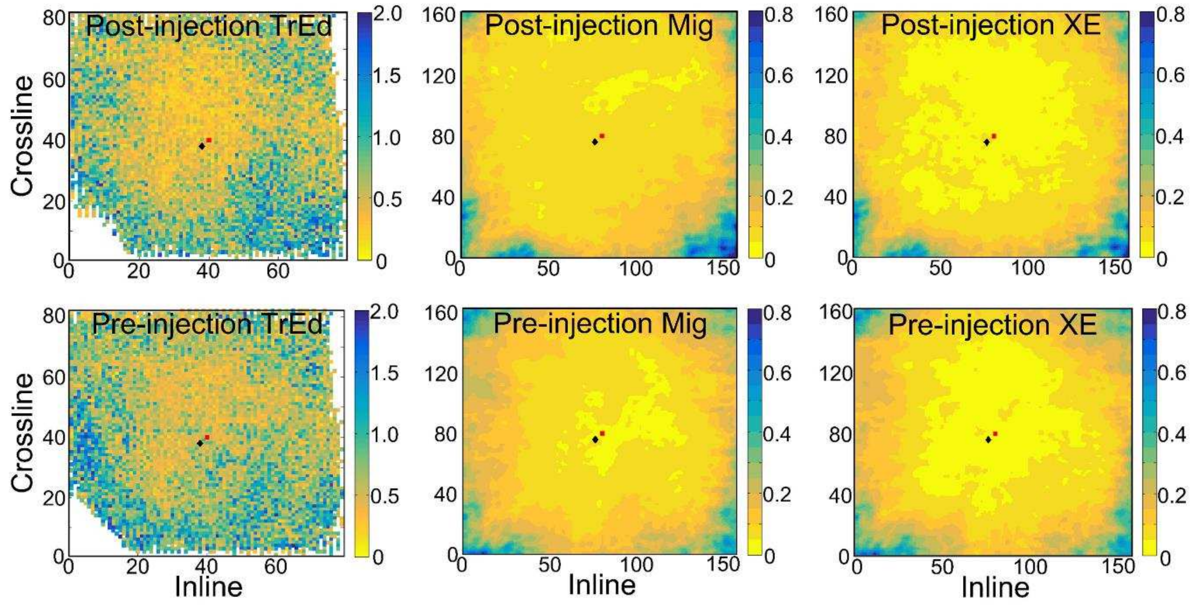

Figure 10: Maps of trace-by-trace nRMS computed within the 1800ms to 1900ms window on the post-CO_2-injection (A to C) and Baseline–Monitor 1 pre-CO_2-injection (D to F) stacked traces at different points in the processing flow. Trace edited stacks (A,D), migrated stacks (B,E) and cross-equalised (XE) stacks (C,F). The red square marks the observation well and the black diamond marks the injection well.

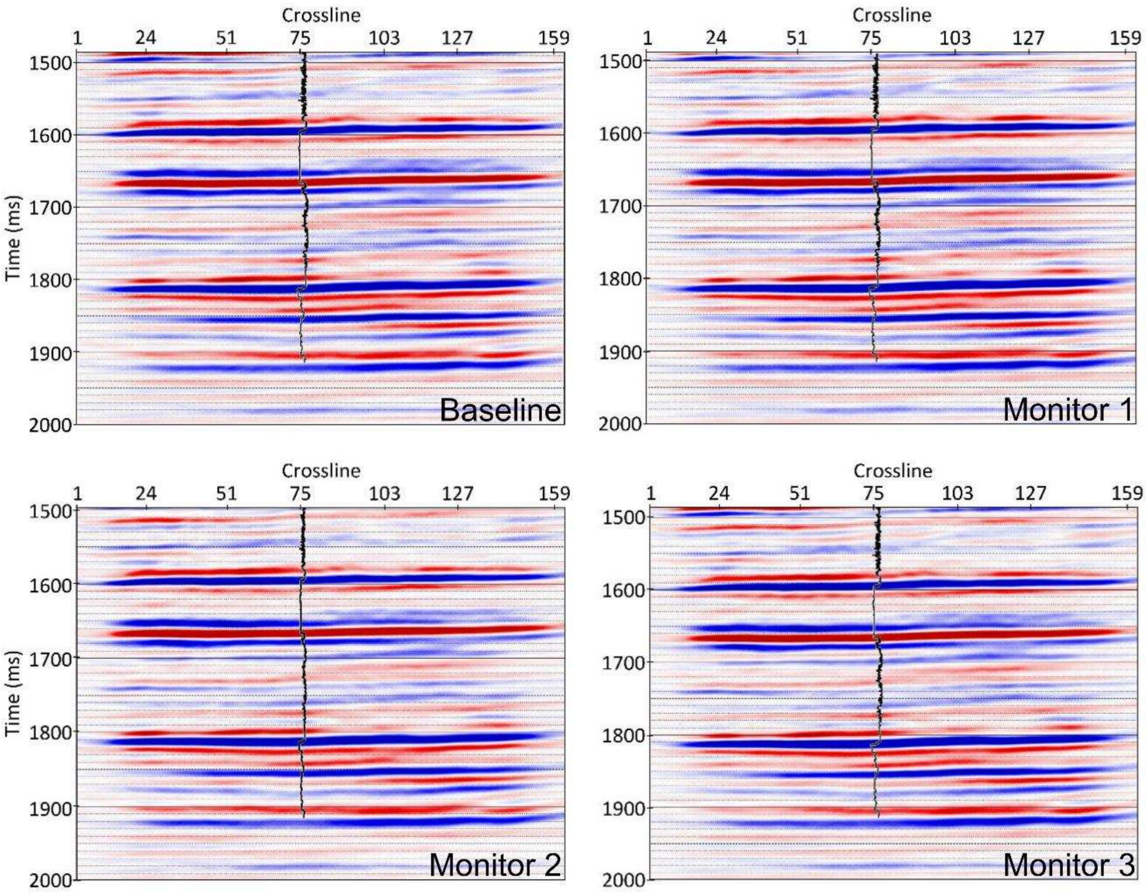

Figure 11: Coincident sections from each vintage of 3D data along an inline (IL76) that intersects the injection well. Superposed is the Vp log. The reservoir horizons between 1800 ms to 1900 ms can be identified by comparison with Figure 3. Note that these data have been converted to zero-phase by applying a phase shift of -140° as compared to the data shown in Figure 3.

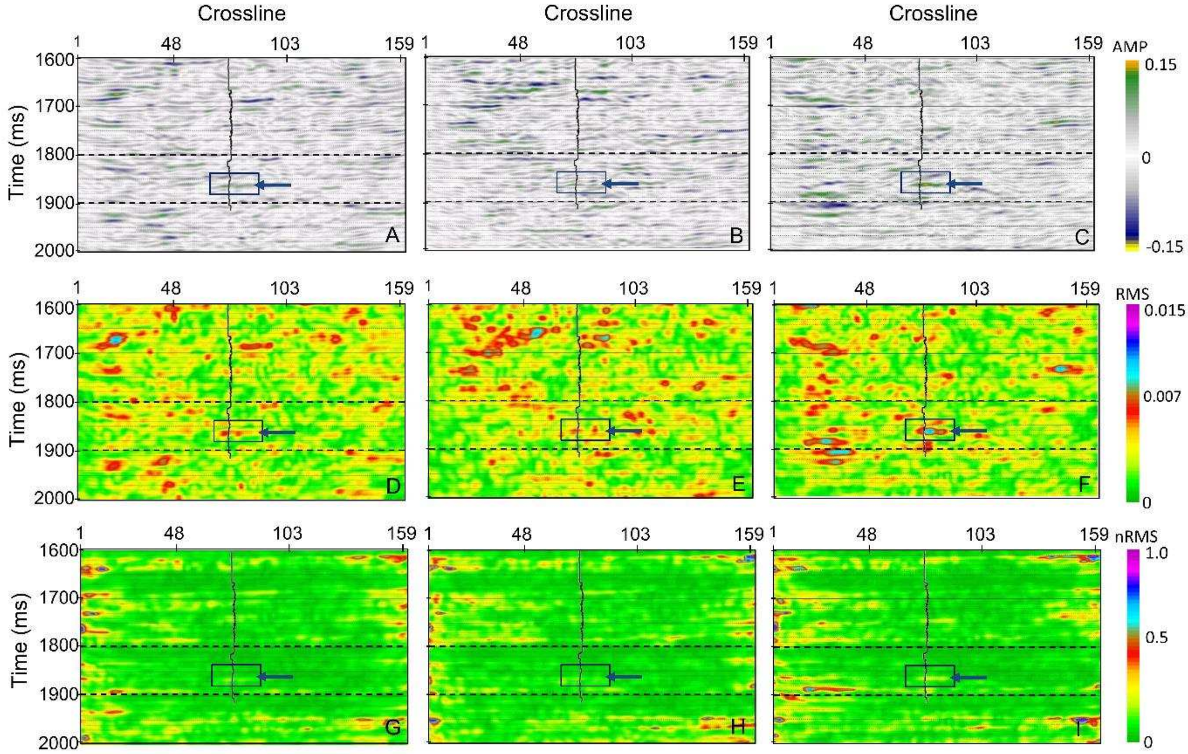

Figure 12: Difference of monitor surveys relative to baseline: Amplitude difference for (A) Monitor 1, (B) Monitor 2, and (C) Monitor 3. RMS amplitude difference for (D) Monitor 1, (E) Monitor 2 and (F) Monitor 3. nRMS amplitude difference for (G) Monitor 1, (H) Monitor 2 and (I) Monitor 3. The sections shown are from the same location as in Figure 11. Note that an amplitude scaling factor of 10 is used here as compared to Figure 11. Superposed is the Vp log. The reservoir is demarked by the black dashed lines. The solid blue box highlights the region within the reservoir (~1840 ms to 1880 ms) with an amplitude anomaly on Monitor 3 (right column) which is not visible on Monitor 1 (left column) or Monitor 2 (middle column).

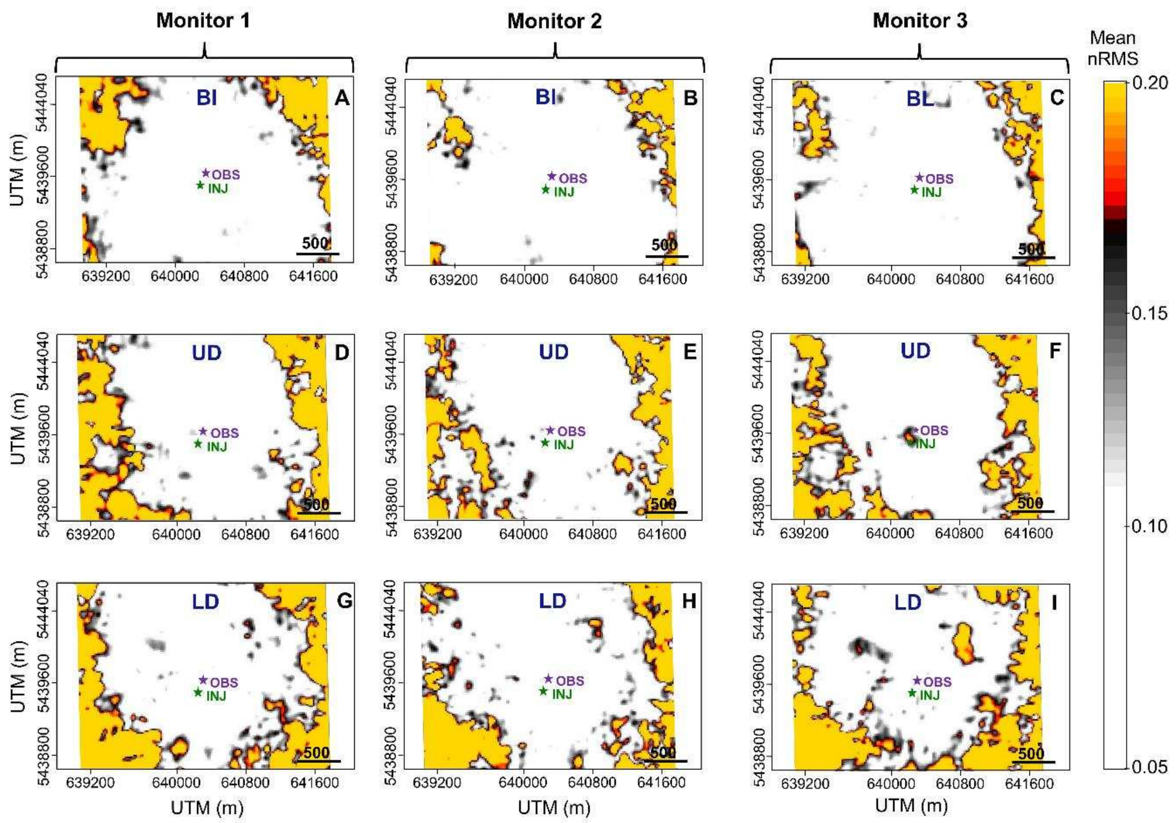

Figure 13: Maps of trace-by-trace mean nRMS difference values determined at 3 levels within the reservoir (1830 ms, 1864 ms, and 1880 ms, from top to bottom, respectively). The values shown are the mean value within a 10 ms window of the 10-ms nRMS. 3x3 smoothing has also been applied. Left column: cross-equalised Monitor 1 difference volumes. Middle column: cross-equalised Monitor 2 difference volumes. Right column: the cross-equalised Monitor 3 difference volumes. The injection (INJ) and observation (OBS) wells are labelled. For scale, the double red circles around the plume (F) have radii of 100 m and 150 m. BI=Black Island; UD=upper Deadwood; LD=lower Deadwood. The use of the non-linear colour scale is designed to 1) exclude amplitudes (nRMS < 0.11) that are below the time-lapse noise threshold, and 2) to emphasize amplitudes that are significantly above the surrounding background levels (nRMS > 0.17).

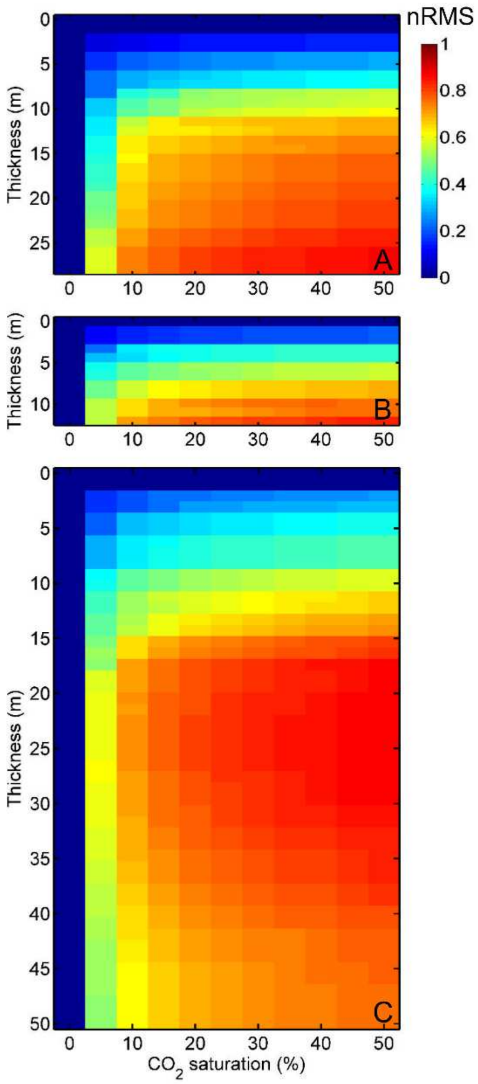

Figure 14: nRMS differences determined for synthetic baseline and monitor traces for perforation zones in (A) Winnipeg Black Island interval, (B) upper Deadwood interval, and (C) lower Deadwood interval. Each point on the maps corresponds to a single CO_2 saturation – layer thickness combination and the amplitude represents the mean nRMS value determined for a 10 ms window. CO_2 saturation varies in 5% increments and layer thickness in 1m increments. The maps were determined using the same Gassmann-based fluid substitution modelling and synthetic seismogram calculation as Roach et al. (2015), but applied to perforation intervals within the injection well.

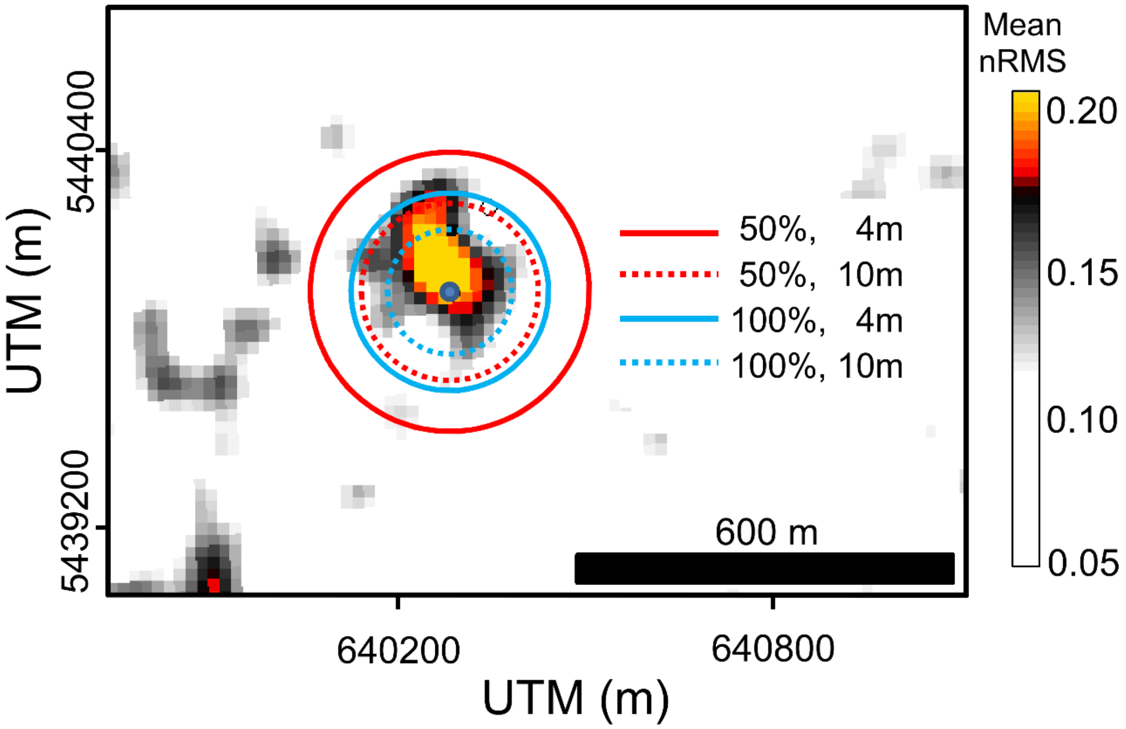

Figure 15: Enlarged portion of the post-injection nRMS map for the upper Deadwood interval from Figure 13F. Superposed are circles representing the area of a hypothetical cylindrical CO_2 plume for different combinations of assumed CO_2 saturation (50% and 100%) and thickness (4 or 10m) within this zone. See the text for further discussion.